Eroglu *Earth, Planets and Space* (2019) 71:26
https://doi.org/10.1186/s40623-019-1002-1

Earth, Planets and Space

FULL PAPER Open Access

Modeling the superstorm in the 24th solar cycle

Emre Eroglu*

Abstract:

The St. Patrick's Day phenomenon is a geomagnetic storm that deserves serious discussion because of its intensity and effectiveness. This study focuses on the St. Patrick's Day storm on March 17, 2015, which is the first big storm of the 24th solar cycle. The data obtained from various spacecrafts observing the ionosphere reveal the reputation and the strength of the storm. The author tries to discuss the event as a whole with all its parameters. Variables of the study are the solar wind parameters and zonal geomagnetic indices. Models with solar wind pressure, proton density and magnetic field may aid in making the dynamic structure of the phenomenon more understandable. The obtained models are able to give the reader an idea of the results even if the storm prediction percentage is low. The author has endeavored to obey the cause–effect relationship without ignoring the physical principles when establishing mathematical models. Despite the fact that the relations between variables have poor correlation or have low statistical significance, in order to introduce the physical point of view they have not been ignored. This study puts forth a new mathematical perspective by discussing and visualizing what happened in the phenomenon.s

Keywords: Mathematical modeling, Zonal geomagnetic indices, Solar wind parameters

Introduction

The St. Patrick's Day geomagnetic storm is one of the most remarkable storms in the 24th solar cycle. The phenomenon has caused serious negative effects on the Earth. One of the reasons that make the storm interesting and important is the magnitude of the storm, and the other one is it has not been forecasted.

If one tries to reveal scientific results about geomagnetic storms, he/she should determine the relationship between solar wind parameters and zonal geomagnetic indices. With these two types of variables, the model may be established and the storm can be discussed provided that it obeys physical principles. The zonal geomagnetic indices, which are caused by solar parameter variables such as magnetic field, electric field, dynamic pressure, proton density due to the storm, have been in use since ancient times. Based on these variables, scientists can characterize the magnetosphere (Mayaud 1980; Fu et al. 2010a, b; Rathore et al. 2014). The geomagnetic storms, which have three phases including a sudden commencement, a main phase and a recovery phase, are one of the most important actions involving dynamic structures (Akasofu 1964; Burton et al. 1975). The storm reaction of the dynamic structure starts with coronal mass ejection (CME). During the CME pulse, large solar plasma clouds with an average speed of 800 km/s seriously affect magnetosphere, leaving its place to define the magnetic activity indices that determine the reflex of the geomagnetic storm. Magnetic activity indices such as AE (auroral electrojet), ap, Kp (planetary index) and Dst (disturbance storm time) are described to specify the effects of the geomagnetic storm. AE is the hourly auroral electrojet index, ap is the planetary index derived from Kp, and Kp is the quasi-logarithmic planetary index. The author utilizes hourly versions of AE and Kp indices. Dst, which exhibits the level of the magnetic storm (Hanslmeier 2007), is the hourly index related to the ring current. Kp, ap and Dst indices are generally used to define a magnetic storm (Mayaud 1980; Kamide et al. 1998; Joshi et al. 2011; Elliott et al. 2013). The St. Patrick's Day storm started on March 17 with CME. CME usually causes

*Correspondence: eroglumre@gmail.com
Department of Mathematics, Kirklareli University, Kayali Campus, 39100 Kirklareli, Turkey

sudden increases in solar wind dynamic pressure. The reason for the formation of CMEs is the regional reconnections in the solar corona (Lin and Forbes 2000). These reconnections are the result of magnetic-field-line merging (Fu et al. 2011, 2012, 2013a, b, 2015, 2017). During the eruption, the light isotopes and plasmas in the solar corona are spread throughout the solar magnetic field. The charged particles interact with the Earth's magnetic field, causing intermittent disturbance of the ionosphere and magnetosphere (Fu et al. 2011, 2012, 2013b). Some observational (Zic et al. 2015; Manoharan et al. 2017; Subrahmanya et al. 2017) evidences suggested that the ionospheric disturbance dynamo had a significant effect on storm-time ionospheric electric fields at medium and low latitudes (Blanc and Richmond 1980). The CME leads directly to the change in solar wind parameters (Gonzalez et al. 1999).

Mathematical models give information to researchers about variables and their relationships, even if they are in different scientific areas (Ak et al. 2012; Celebi et al. 2014; Eroglu et al. 2016). In addition, they should give clues about the behavior of the variables under different circumstances and varied plasma-dense medium. Investigation of the evolution of dense plasmas over time cannot be limited to a single event. Because of their dynamic structures, establishing models will benefit scientists (Sibeck et al. 1991). Dynamic models have been used in many previous studies to describe global loading and unloading operations in storms (Burton et al. 1975; Baker et al. 1990; Dungey 1961; Gonzalez et al. 1994; Sugiura 1964; Temerin and Li 2002; Tsyganenko et al. 2003; Fu et al. 2014). Previously applied models can also be seen in this storm. For example, Wu and Leping (2016) have applied Gilmore et al. (2002) formula to St. Patrick's Day storm for Dst and B_z.

The effects of the storm in all longitudinal sectors are characterized using spherical and regional electric current. Estimation of ionospheric current density can minimize the negative effects of substorm activity. The improvement of high-latitude ionospheric convection models aids in predicting substorm events (Chen et al. 2016). The effects of the magnetospheric convection electric field and the disturbing dynamo electric field at low latitudes were previously investigated (Fu et al. 2010a, b; Nava et al. 2016). The magnetic field oscillations of the Earth are seen at the same time in the Asian, African and American sectors during the southward orientation of the B_z component in the interplanetary magnetic field. The ionospheric irregularities at the high latitudes associated with auroral activities have been studied by Cherniak and Zakharenkova (2015).

The St. Patrick's Day geomagnetic storm (Astafyeva et al. 2015; Cherniak et al. 2015; Baker et al. 2016; Gvishiani et al. 2016; Nayak et al. 2016) has been widely studied during the past 2 years. It is necessary to understand the complex effects of the geomagnetic storm and predict the event based on the solar wind and IMF parameters. We focus on the variables of the phenomenon and discuss mathematical models. Binary linear models have difficulty in explaining the exact relationship between variables. Nevertheless, the presentation of these models is important (Eroglu 2018). Weak correlation inspires scientists to search for linear and nonlinear models. All approaches have exact obedience cause–effect relationship, and the causality principle governs linear and nonlinear models (Tretyakov and Erden 2008; Eroglu et al. 2012). The cause–effect relation should be thought of as an inseparable duo. The solar wind plasma parameters [the magnetic field (B_z), the electric field (E), the solar wind dynamic pressure (P), the proton density (N), the flow velocity (v) and the temperature (T)] of the phenomenon are the "cause." The zonal geomagnetic indices (Dst, ap, Kp and AE) of the storm are the "effect."

This paper uses the solar wind parameters (P, v, E, T, N, B_z) and zonal geomagnetic indices (Dst, AE, Kp, ap). The author utilizes hourly versions of AE and Kp indices. In order to better interpret the first intense (-250 nT $\leq$ Dst < -100 nT) storm of the 24th solar cycle (March 17, 2015), solar wind parameters and zonal indices are analyzed in depth and linear and nonlinear models are established. The models support the previous work conducted by Eroglu (2018).

In "Data" section the solar parameters, zonal geomagnetic indices and a five-day distribution of variables are presented. In "Mathematical modeling" and "Conclusion" sections, the analyses are performed and discussion is given, respectively.

Data

Space Physics Environment Data Analysis Software (SPEDAS) is used in this research. Analysis software data are IDL based. It is accessible at the link below: http://themis.igpp.ucla.edu/software.shtml. The hourly OMNI-2 Solar Wind and IMF parameter data are accessible online. In addition, the AE and Dst indexes are taken from World Data Center for Geomagnetism, Kyoto, by using SPEDAS. Kp and ap are taken from NGDC by using SPEDAS with CDA Web Data Chooser (space physics public data). For March 2015 severe storm, solar wind dynamic pressure, IMF, electric field, flow speed and proton density were recorded in the OMNI hourly data. Geomagnetic storms are classified according to the intensity of the Dst index (Loewe and Prölss 1997). If the Dst index

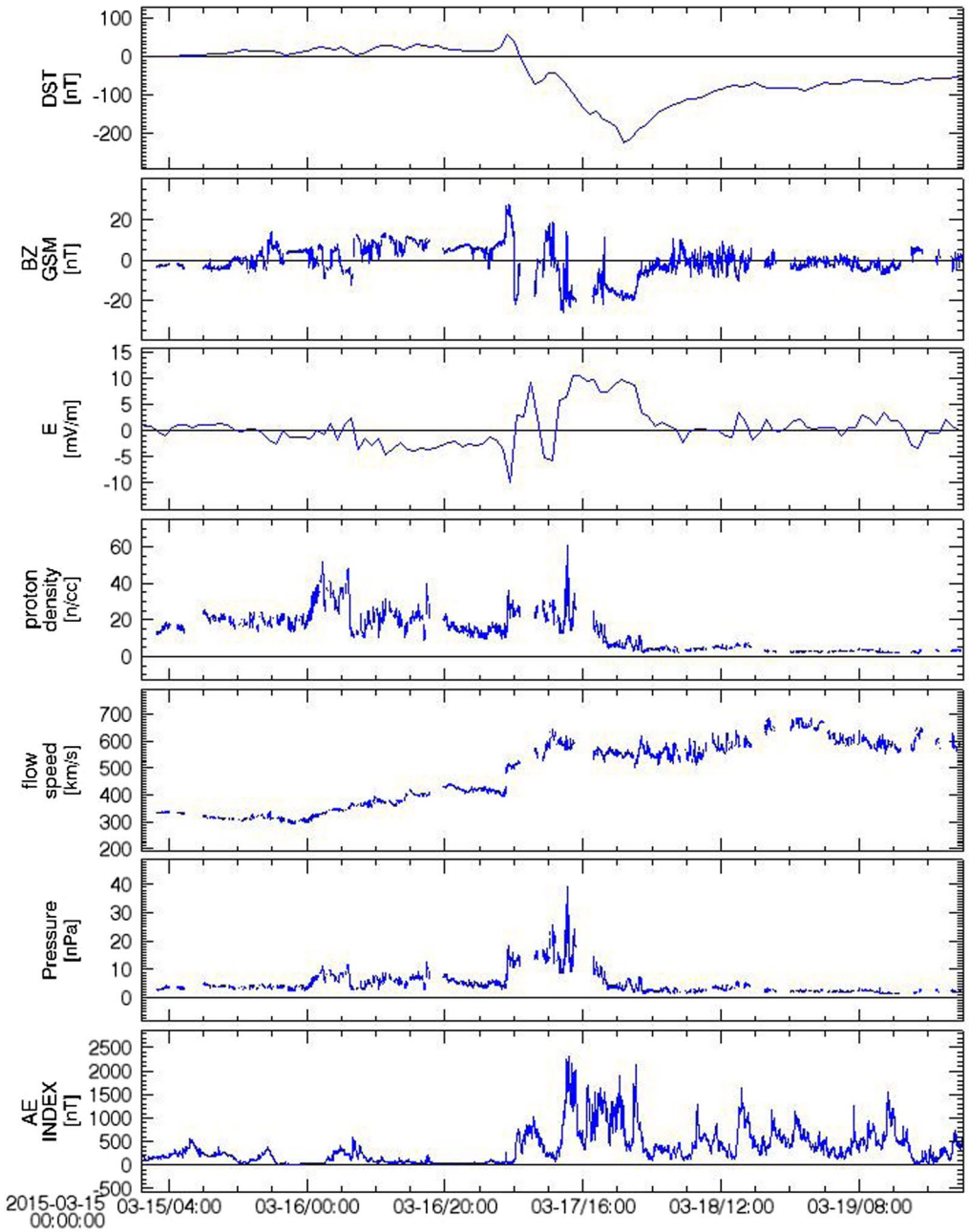

Fig. 1 From top to bottom the parameters shown are Dst index, B_z magnetic field (nT), E electric field (mV/m), proton density N (1/cm^3), solar wind dynamic pressure P (nPa), flow speed v (km/s) and auroral electrojet AE (nT) index for March 15–19, 2015 (from NASA NSSDC OMNI data set). The characteristic storm at the intense level (Dst = − 223 nT) on March 17, 2015, has been analyzed. Figure 1 shows the OMNI data set from 00 UT March 15, 2015, to 00 UT March 19, 2015. The plot interval covers the storm day (March 17, 2015), 2 days before and 2 days after (120 h) the storm

is between − 50 and − 30 nT this indicates a weak storm. If it is between − 100 and − 50 nT this indicates a moderate storm. The Dst index between − 200 and − 100 nT indicates a strong (intense) geomagnetic storm.

The characteristic storm at the intense level (Dst = − 223 nT) on March 17, 2015, has been analyzed. Figure 1 shows the OMNI data set from 00:00 UT on March 15, 2015, to 00:00 UT on March 19, 2015. The plot interval covers the storm day (March 17, 2015), 2 days before and 2 days after the storm (120 h). The St. Patrick's Day storm started on March 17 with CME. The solar wind pressure (P) suddenly rose to one of the highest values of 17.91 nPa

(min.: 1.68; max.: 20.76 nPa), the magnetic field component (B_z) reached its maximum value of 20.1 nT, and the proton density (N) increased to 38.5 1/cm^3, one of its greatest values (min.: 2.7; max.: 40.1 cm^{-3}) between 04:00 and 05:00 UT on March 17. The plasma flow speed (v) rose to 609 km/s 5 h later. It may be useful to observe variables at the maximum or minimum values before reviewing the literature. During the St. Patrick's Day storm, the Dst index reached the minimum value of − 223 nT and the geomagnetic aurora electrojet index (AE) increased to reach its maximum value of 1570 nT. The magnetic field component of B_z decreased to − 18 nT, and ap index increased to 179 nT. The aurora appears in both hemispheres.

The parameters shown in Dst index, B_z magnetic field (nT), E electric field (mV/m), proton density N (1/cm^3), solar wind dynamic pressure P (nPa), flow speed v (km/s) and auroral electrojet AE (nT) for March 15–19, 2015, are obtained from NASA NSSDC OMNI data set.

Figure 1 is specifically described as follows. On March 17, 2015, at 22:00 (UT), when Dst is at its minimum (− 223 nT), B_z component increases to − 16.5 nT and the electric field E reaches 5.2 mV/m. Meanwhile, ap index reaches its maximum value 179 nT by increasing, proton density N is 8.6 1/cm^3, plasma flow speed v reaches one of the highest values of 558 km/s, and AE index catches 457 nT.

On March 17, 2015, at 14:00 (UT), when B_z component is minimum (− 18.1 nT), Dst index continues to decrease toward the minimum, the electric field E reaches its own maximum value of 10.5 mV/m, AE index reaches its own maximum value of 1570 nT, ap index reaches its maximum value 179 nT, and flow pressure P takes its own one of the maximum values of 16.7 nPa.

On March 17, 2015, at 05:00 (UT), when B_z component is maximum (20.1 nT), the electric field reaches its minimum value of − 9.9 mV/m, proton density N takes its own one of the maximum values of 38.5 1/cm^3, AE index decreases and falls to one of the minimum values of 50 nT, and ap index continues to increase. As this happens Dst index reaches its maximum value 56 nT.

Table 1 Descriptive analysis

	N	Minimum	Maximum	Mean	SD
B_z (nT)	120	− 18.1	20.1	− .317	6.8809
T (K)	120	21,425	912,227	142,900.23	162,135.845
N (1/cm^3)	120	2.7	40.1	14.110	9.6623
v (km/s)	120	298	683	485.23	123.119
P (nPa)	120	1.68	20.76	5.6173	4.46443
E (mV/m)	120	− 9.97	10.57	.5708	3.54970
Kp	120	3	77	37.50	19.355
Dst (nT)	120	− 223	56	− 43.40	63.249
ap (nT)	120	2	179	39.60	48.606
AE (nT)	120	17	1570	359.60	330.776

Mathematical modeling

The descriptive analysis values of the geomagnetic storm on March 2015 are displayed in Table 1. The reason for applying the descriptive analysis is to control the change interval of the variables and to acquire an idea about the standard deviations. The effect of the variable with a high standard deviation will be reduced. Accordingly, the most powerful variables statistically are P, E, N, B_z, ap, respectively. It is expected that these variables will shape the storm. However, because of the causality principle and the cause–effect relationship, solar parameters are the causes and zonal geomagnetic indices are the results of the storm. The instant correlation samples between each coefficient of the storm are shown in Table 2. Pearson's correlation analysis is a parametrical statistical method which shows the direction, degree and importance of the relationship between variables. The correlation analysis is

Table 2 Pearson's correlation matrix for the storm variables

	B_z (nT)	T (K)	N (1/cm^3)	v (km/s)	P (nPa)	E (mV/m)	Kp	Dst (nT)	ap (nT)	AE (nT)
B_z (nT)	1	.038	.171	− .316**	− .165	− .889**	− .580**	.618**	− .712**	− .687**
T (K)		1	− .133	.511**	.378**	.084	.407**	− .224*	.241**	.244**
N (1/cm^3)			1	− .682**	.627**	− .130	− .274**	.658**	− .068	− .277**
v (km/s)				1	.060	.339**	.702**	− .742**	.483**	.582**
P (nPa)					1	.272**	.416**	.060	.532**	.271**
E (mV/m)						1	.648**	− .616**	.783**	.757**
Kp							1	− .755**	.887**	.767**
Dst (nT)								1	− .678**	− .655**
ap (nT)									1	.754**
AE (nT)										1

* and ** Correlations are significant at the 0.05 level (two-tailed) and at the 0.01 level (two-tailed), respectively

Table 3 KMO and Bartlett's test

Kaiser–Meyer–Olkin measure of sampling adequacy	.762
Bartlett's test of sphericity	
Approx. Chi square	1385.342
df	45
Sig.	.000

a complementary method of regression analysis. While the value between the two variables approaches ± 1, the relationship is strengthening. Physically, in this storm, the models in which take place B_z with ap, Dst, AE and T with v and N with v, P and v with Kp, Dst, AE and P with ap and E with Kp, Dst, ap, AE may be considered as preferential.

KMO and Bartlett's test tables (Table 3) reveal the suitability of the data for factor analysis and show the strength of the relationship between variables. The Kaiser–Meyer–Olkin measure of sampling adequacy is a statistic and shows the commensurate of the variance in data that can be caused by main factors. High values (close to 1.0) imply that data are appropriate for a satisfactory factor analysis method. If the test value of variables is appropriate to the method, they exhibit a normal distribution. In order to deny the hypothesis H_0 (null hypothesis), the significance of the test should be less than 0.05. The attitudes of the data released as a result of a physical phenomenon can be determined by this test. If the data of the physical event indicate normal distribution, the variables show how they can be coordinated with each other and with the event. Thus, the linear or nonlinear relations can be discussed and models can be argued with obeying the mathematical approaches. As can be seen from Table 3, the variable set of this storm is suitable for factor analysis.

Factor analysis is used with the principle component analysis and varimax with Kaiser normalization for the rotation (converged in 3 iterations) to divide the variables into subgroups and to distinguish those who have the highest contribution to the event. In this analysis, which does not include composite variables, each variable is handled separately. The variables are examined in a more specific (by heap) way with basic component analysis. In Table 4, when the ten variables are substituted into the data reduction method, three maximum eigenvalues of the covariance matrix describe 88% of the total change, which means that it can be explained by modeling the 88% of the phenomenon with the variables at hand.

Varimax with Kaiser normalization method for the rotation matrix examines the linear grouping of variables of the event. The method approaching each variable as a factor indicates the contribution and weight of these factors in the linear clustering. Table 5 summarizes these weights.

Hence, these models can be written as follows with factor weights from Table 5.

$$\begin{aligned}\text{Axes } 1 = &-(0.920)B_z - (0.001)T - (0.141)N \\ &+ (0.400)v + (0.315)P + (0.938)E \\ &+ (0.766)\text{Kp} - (0.702)\text{Dst} \\ &+ (0.887)\text{ap} + (0.828)\text{AE}\end{aligned}$$

$$\begin{aligned}\text{Axes } 2 = &(0.069)B_z + (0.054)T + (0.956)N \\ &- (0.518)v + (0.805)P + (0.012)E \\ &- (0.070)\text{Kp} + (0.543)\text{Dst} \\ &+ (0.137)\text{ap} - (0.115)\text{AE}\end{aligned}$$

Figure 2 illustrates the physical scattering of Dst, ap and AE zonal geomagnetic indices according to B_z, P, v, N solar wind parameters. In this work, the solar wind

Table 4 Total variance explained

Component	Initial eigenvalues			Extraction sums of squared loadings		
	Total	% of variance	Cumulative %	Total	% of variance	Cumulative %
1	5.352	53.515	53.515	5.352	53.515	53.515
2	2.049	20.487	74.002	2.049	20.487	74.002
3	1.432	14.325	88.327	1.432	14.325	88.327

Table 5 Rotated component matrix

Component	B_z (nT)	T (K)	N (1/cm^3)	v (km/s)	P (nPa)	E (mV/m)	Kp	Dst (nT)	ap (nT)	AE (nT)
1	−.920	−.001	−.141	.400	.315	.938	.766	−.702	.887	.828
2	.069	.054	.956	−.518	.805	.012	−.070	.543	.137	−.115

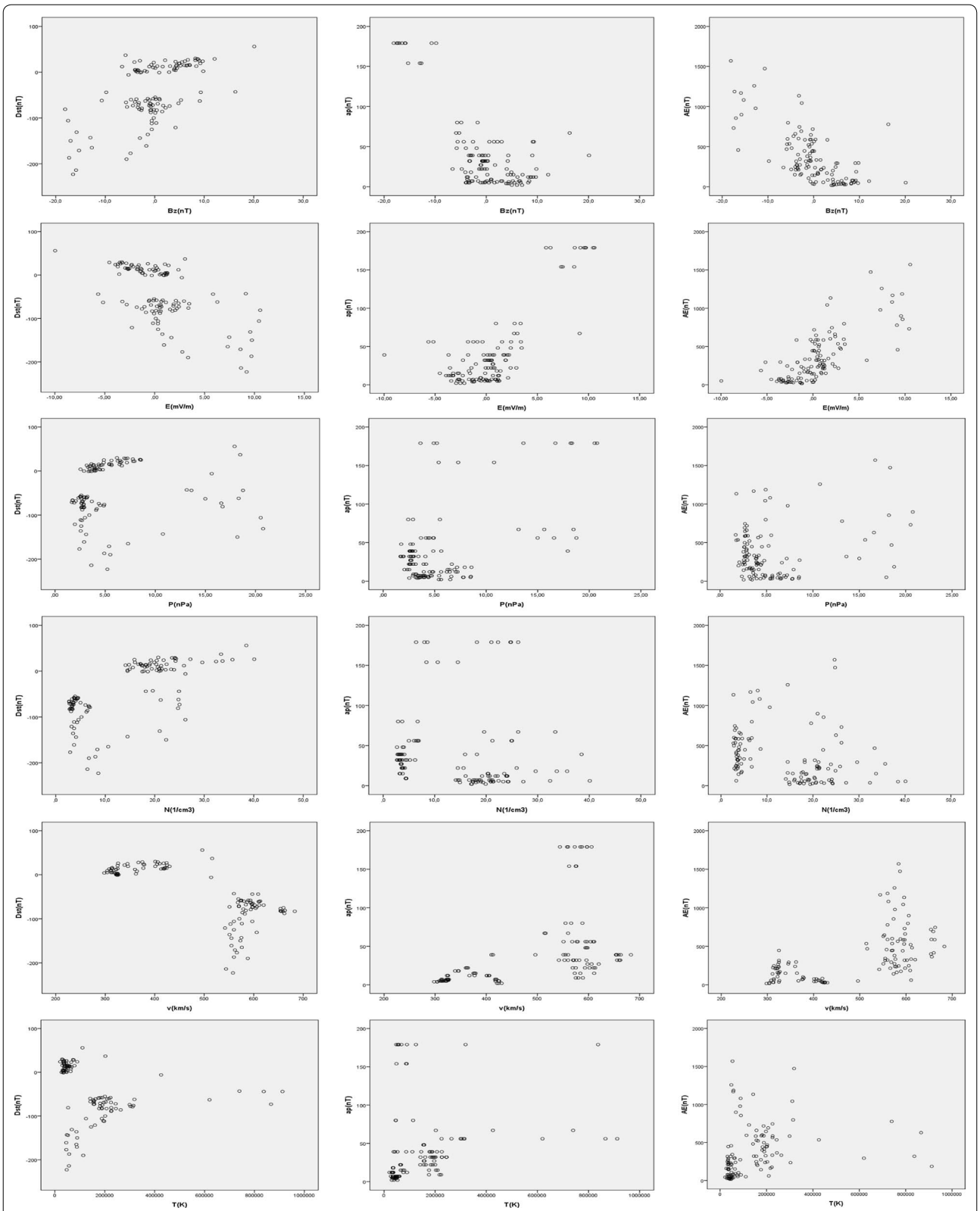

Fig. 2 Appearance between Dst, ap, AE indices and B_z, E, P, N, v, T solar wind parameters. Relation between zonal geomagnetic indices (Dst, ap and AE) and solar wind parameters (magnetic field component (B_z), the electric field (E), dynamic pressure (P), proton density (N), flow velocity (v), temperature (T)) can be seen in Fig. 2. The relationships in the correlation are visualized

propagation time from bow shock to Earth is not taken into account when Dst, ap and AE data from ground stations are used. As the time is too short to take these into account, one can find in Fig. 2 only the magnitudes of the values of B_z, E, P, N, v, T solar wind parameters and Dst, ap, AE zonal geomagnetic indices, no matter how and when these arose with respect to each other.

According to Fig. 2, the physical reaction of zonal geomagnetic indices to the change in solar wind parameters in the storming process can be summarized as follows. The response of Dst to the magnetic field B_z component, the electric field (E), proton density (N) and temperature (T) is linear, and the response to the dynamic pressure (P) and flow speed (v) is nonlinear. While the response of the ap index to B_z, electric field, flow speed and temperature is linear, its response to dynamic pressure and proton density is nonlinear. While the response of the AE index to B_z, electric field, dynamic pressure and temperature is linear, its response to proton density and flow speed is nonlinear.

Linear and nonlinear model

The regression model is:

$$y_i = f_i(x, b) + \varepsilon_i = \sum_{j=1}^{n} b_j x_j + \varepsilon_i$$

where y_i is dependent variable, x_j is n-dimensional independent variable, and ε_i is error. $f_i(x, b)$ is called the *expectation function* for the regression model.

The sample covariance s_{jk}^2 is:

$$s_{jk}^2 \equiv \frac{\frac{1}{n-1}\sum_{i=1}^{n}\left[\frac{1}{\sigma_i^2}\left(x_{ij}-\bar{x}_j\right)\left(x_{ik}-\bar{x}_k\right)\right]}{\frac{1}{n}\sum_{i=1}^{n}\left(\frac{1}{\sigma_i^2}\right)}$$

where j, $k=1$, 2; σ_i^2 is the standard deviation; n is the number of data points; and $\bar{x}_j$ is

$$\bar{x}_j \equiv \frac{\sum_{i=1}^{n}\left(\frac{x_{ij}}{\sigma_i^2}\right)}{\sum_{i=1}^{n}\left(\frac{1}{\sigma_i^2}\right)}.$$

The sample variance is given by $s_j^2 \equiv s_{jj}^2$. The correlation coefficient can be expressed in terms of $r_{jk} \equiv \frac{s_{jk}^2}{s_j s_k}$. Square of multiple correlation coefficient R^2 is:

$$R^2 \equiv \sum_{j=1}^{n}\left(b_j \frac{s_{jy}^2}{s_y^2}\right) = \sum_{j=1}^{n}\left(b_j \frac{s_j}{s_y} r_{jy}\right).$$

R^2 is the percentage of the event defined by the model. The closer the R^2 is to one (1) in the established model, the greater the percentage of the model's description of the event is (Freund 1979; Saba et al. 1997).

Before discussing the binary relations of the zonal geomagnetic indices governed by the solar wind parameters, it would be appropriate to see the linear compositions of the indices. According to independent variables (solar wind parameters), the linear compounds of the dependent variables Dst and ap (zonal geomagnetic indices) are given in Tables 6, 7, 8 and 9, respectively. The coefficients can be seen from the tables. This table (Table 6) demonstrates how much of the residuals are explained by the variables in the linear regression model. One may realize that regression coefficients are

Table 6 ANOVA (analysis of variance)

Model	Sum of squares	df	Mean square	*F*	Sig.
Regression	131237.711	4	32,809.428	26.445	.000
Residual	83,124.164	67	1240.659		
Total	214,361.875	71			

Table 7 Regression coefficients

Model	Unstandardized coefficients		Standardized coefficients	*t*	Sig.
	B	SE	Beta		
(Constant)	− 244.925	73.544		− 3.330	.001
B_z (nT)	3.497	.670	.471	5.217	.000
N (1/cm3)	10.321	2.396	1.617	4.308	.000
P (nPa)	− 11.814	3.457	− 1.201	− 3.417	.001
v (km/s)	.256	.123	.265	2.078	.042

Table 8 ANOVA (analysis of variance)

Model	Sum of squares	df	Mean square	*F*	Sig.
Regression	163,844.271	3	54,614.757	90.643	.000
Residual	40,971.729	68	602.525		
Total	204,816.000	71			

Table 9 Regression coefficients

Model	Unstandardized coefficients		Standardized coefficients	*t*	Sig.
	B	SE	Beta		
(Constant)	24.093	4.244		5.676	.000
E (mV/m)	4.653	1.477	.349	3.151	.002
P (nPa)	3.771	.554	.392	6.801	.000
B_z (nT)	− 2.769	.780	− .382	− 3.551	.001

significant. Table 7 shows the model of Dst index as: $\mathrm{Dst} = -(244.925) + (3.497)B_z + (10.321)N - (11.814)P + (0.256)v$, where multiple determination coefficient R is 0.782.

Table 8 indicates that the model is significant, while Table 9 shows that the ap index is: $\mathrm{ap} = (24.093) + (4.653)E + (3.771)P - (2.769)B_z$, where multiple determination coefficient R is 0.894.

Physically, the magnetospheric activity is nonlinearly proportional to the proton density (N) and plasma flow speed (v) and linearly proportional to the interplanetary magnetic field (IMF) (Temerin and Li 2006; Agopyan 2010). Changes in solar wind pressure and CME cause nonlinear behavior, fluctuations and changes in the density of particles. The serious (> 10 nT) orientation of the B_z component of the magnetic field to the southward for more than a few hours causes depression in the Dst and gets Dst directed to the negative direction. This depression on the Dst demonstrates a severe storm. Visualizing the response of such a storm to the solar wind parameters (especially B_z component) of the Dst index will give the reader a clearer idea. The linear and nonlinear models between the Dst, ap, AE indices and B_z are shown in Figs. 3, 4, 5 and Tables 10, 11, 12, respectively. The low correlation coefficients in these models should not be overlooked. Statistically, these are generally middle levels of models.

We know the importance of linear relationship between Dst and B_z step by step (Kane 2010). In addition to this approach, it is useful to investigate the relationship between ap and B_z, and between AE and B_z using both linear and nonlinear models. Table 10 and Fig. 3 display the linear and quadratic relationships of the magnetic field component B_z with the Dst index. $\mathrm{Dst} = -(41.602) + (5.677)B_z$ where R is 0.618, and $\mathrm{Dst} = -(38.016) + (5.418)B_z - (0.078)B_z^2$ where R is 0.625.

In Table 11 and Fig. 4, the linear and nonlinear relationships between the magnetic field component B_z and the ap index are presented. $\mathrm{ap} = (38.007) - (5.029)B_z$ where R is 0.712, and $\mathrm{ap} = (22.542) - (3.913)B_z + (0.336)B_z^2$ where R is 0.896. Mathematically, the height level of the nonlinear correlation with the B_z component and ap index should not be overlooked.

In Table 12 and Fig. 5, the linear and nonlinear relationships between the magnetic field component B_z and the AE index are presented. $\mathrm{AE} = (349.146) - (33.012)B_z$ where R is 0.687, and $\mathrm{AE} = (299.596) - (29.434)B_z + (1.077)B_z^2$ where R is 0.733.

Physically, fluctuations in the magnetic field indicate similar linear effects in flow pressure (P) and proton density (N), while ap index responds to these fluctuations nonlinearly. This nonlinear relationship and model are shown in Table 11 and Fig. 4. The nonlinear model is in the form of $P = a + b\ln \mathrm{ap} + cN$, where a, b, c are constants. The analysis of variance values of the model are shown in Table 13. The magnitudes of coefficients are $a = -7.209$, $b = 2.460$ and $c = 0.376$. Table 14 shows that all parameter estimation is in the confidence

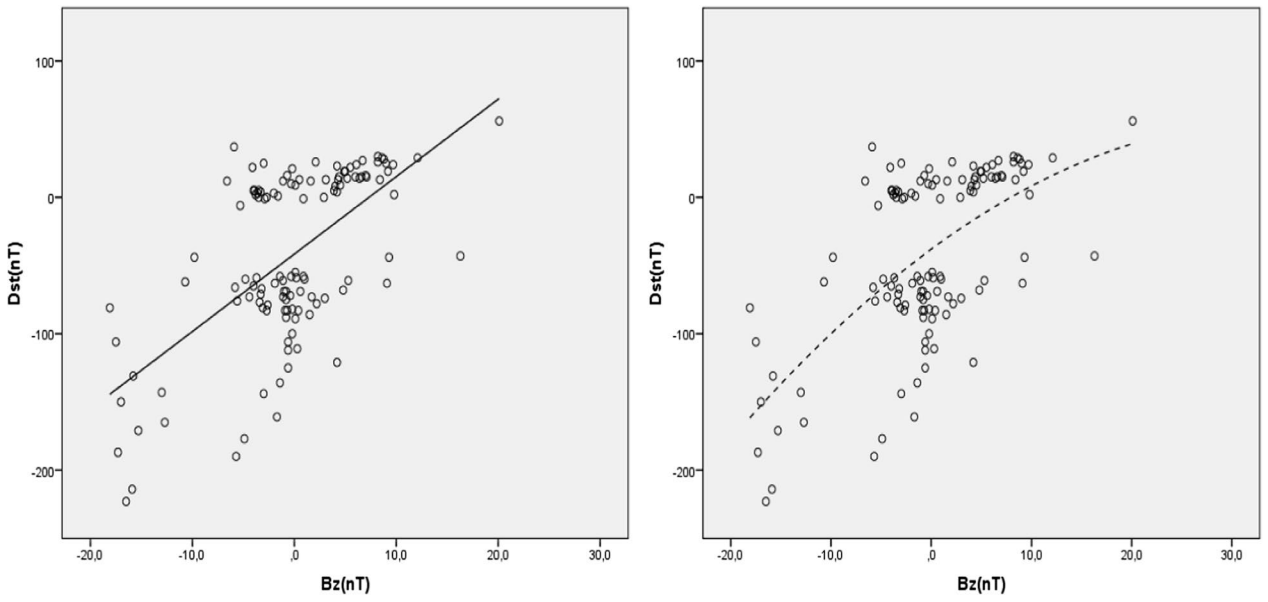

Fig. 3 Linear and quadratic relation of Dst and B_z. In Fig. 3, the linear and quadratic relationships of the magnetic field component B_z with the Dst index are shown

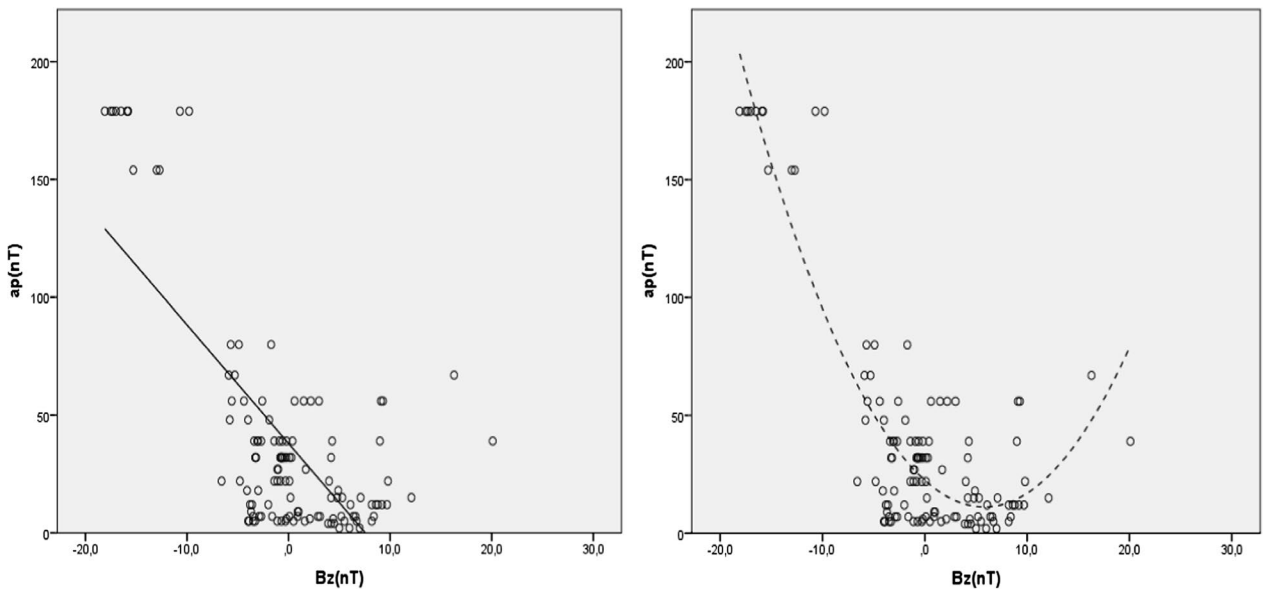

Fig. 4 Linear and quadratic relation between ap and B_z. In figure, the nonlinear relationship between the magnetic field component B_z and the ap index can be seen

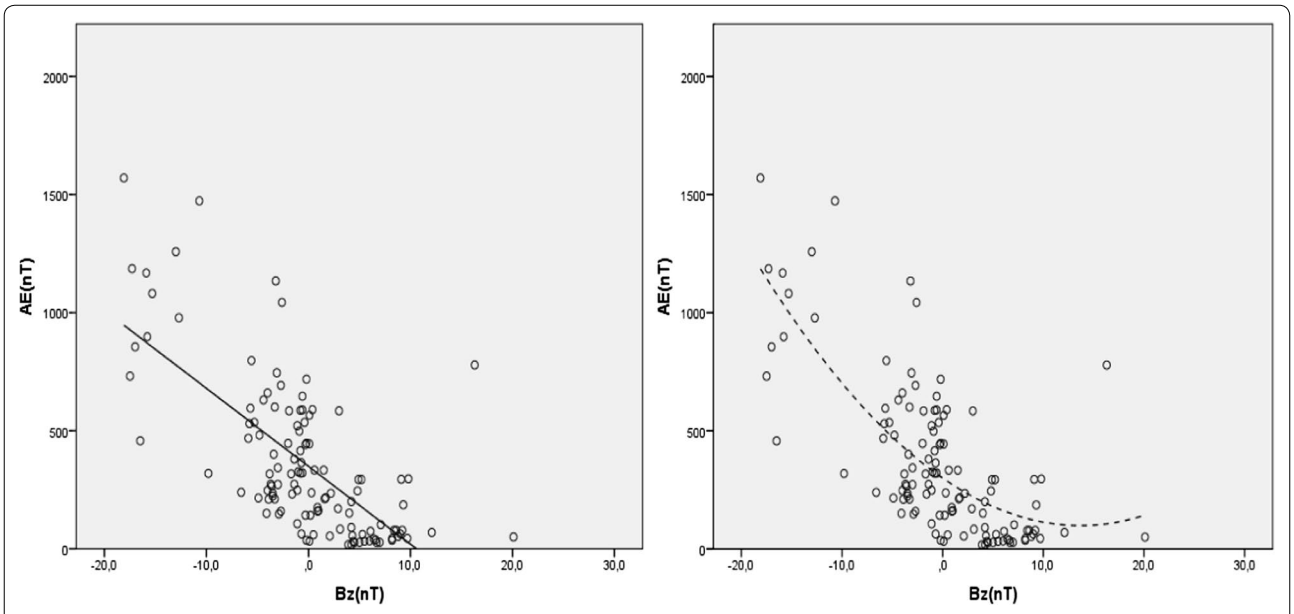

Fig. 5 Linear and quadratic relation of AE and B_z. In figure, the nonlinear relationship between the magnetic field component B_z and the AE index can be seen

interval of 95%. The model explaining this storm with 75.2% accuracy is

$$P = -(7.209) + (2.460)\ln \text{ ap} + (0.376)N.$$

We believe that this nonlinear mathematical model allows a unique expression of pressure and density for plasma-dense medium (underground or atmosphere).

Table 10 Regression coefficients

	Unstandardized coefficients		Standardized coefficients	*t*	Sig.
	B	SE	Beta		
B_z (nT)	5.677	.665	.618	8.532	.000
(Constant)	− 41.602	4.565		− 9.114	.000
	Unstand. coeff.		Stand. coeff.	*t*	Sig.
	B	SE	Beta		
B_z (nT)	5.418	.691	.589	7.846	.000
B_z^2 (nT)	− .078	.058	− .101	− 1.344	.081
(Constant)	− 38.016	5.274		− 7.209	.000

Table 11 Regression coefficients

	Unstandardized coefficients		Standardized coefficients	*t*	Sig.
	B	SE	Beta		
B_z (nT)	− 5.029	.457	− .712	− 11.014	.000
(Constant)	38.007	3.132		12.134	.000
	Unstand. coeff.		Stand. coeff.	*t*	Sig.
	B	Std. Err	Beta		
B_z (nT)	− 3.913	.302	− .554	− 12.970	.000
B_z^2 (nT)	.336	.025	.567	13.273	.000
(Constant)	22.542	2.304		9.786	.000

Table 12 Regression coefficients

	Unstandardized coefficients		Standardized coefficients	*t*	Sig.
	B	SE	Beta		
B_z (nT)	− 33.012	3.217	− .687	− 10.262	.000
(Constant)	349.146	22.066		15.823	.000
	Unstand. coeff.		Stand. coeff.	*t*	Sig.
	B	SE	Beta		
B_z (nT)	− 29.434	3.148	− .612	− 9.350	.000
B_z^2 (nT)	1.077	.264	.267	4.075	.000
(Constant)	299.596	24.039		12.463	.000

Conclusion

The St. Patrick's Day geomagnetic storm is the most severe storm in the 24th solar cycle. Every model that can be established about the storm should be meticulously analyzed. In particular, the mathematical models involving magnetic field, solar wind pressure and proton density give ideas of the dynamic nature of the different plasmatic structures. This study has focused on the March 2015 severe storm by using the St. Patrick's Day severe storm data (120 h). The data have been analyzed mathematically, and the models have been established. The models strictly obeying to physical principles have been consistently introduced in this study as well. These models support the previous studies of the author. The zonal geomagnetic indices produced by solar wind parameters are displayed in the

Table 13 ANOVA (analysis of variance)

Source	Sum of squares	df	Mean squares
Regression	2494.129	3	831.376
Residual	384.379	117	3.285
Uncorrected total	2878.509	120	
Corrected total	1209.483	119	

Table 14 Parameter estimates

Parameter	Estimate	SE	95% Confidence interval	
			Lower bound	Upper bound
a	−7.209	.762	−8.719	−5.700
b	2.460	.189	2.086	2.834
c	.376	.022	.332	.420

correlations based on the cause–effect relationship. Graphs and tables have presented the relationship between zonal geomagnetic indices and solar wind parameters, as well as their interactions with each other. All results are in the 95% confidence interval. Even though some models have discussed the various results of the storm with low precision (statistically), they have been included in this paper for comparison.

Authors' contributions

The manuscript has one author. Data are collected and analyzed by the author. All interpretations and explanations belong to the author. The author read and approved the final manuscript.

Acknowledgements

I thank the NASA CDA Web for OMNI Database (http://themis.igpp.ucla.edu/software.shtml) and Kyoto World Data Center for providing AE index and Dst index. I acknowledge the usage of ap and Kp index from the National Geophysical Data Center. The Dst index and AE data were provided by the World Data Center for Geomagnetism at Kyoto University. I would like to thank Kirklareli University, Professor Ali Yigit, Dereyayla and Akyuz families for their valuable support for this study. I thank Professor Huishan S. Fu for his very helpful comments, corrections and suggestions. I thank Professor Halil Atabay for very supportive corrections.

Competing interests

The author declares no competing interests.

Availability of data and materials

The data used in this article are available at the Data Center of NASA https://omniweb.gsfc.nasa.gov/form/dx1.html

Ethics approval and consent to participate

This study does not require ethical approval.

Funding

We declare no funding.

Publisher's Note

Received: 13 March 2018 Accepted: 17 February 2019
Published online: 01 March 2019

References

Ak N, Eroglu E, Guney I (2012) Statistical analysis of soil heavy metals of Istanbul children playgrounds. Energy Educ Sci Technol Part A 28(2):1151–1158

Akasofu SI (1964) The development of the auroral substorm. Planet Space Sci 12(4):273–282

Agopyan H (2010) İstanbul İyonküresinde Ölçülen Şiddetli Manyetik Fırtına Etkilerine Jeofizikten Bir Örnek. Tubav Bilim Dergisi 3:315 **(in Turkish)**

Astafyeva E, Zakharenkova I, Förster M (2015) Ionospheric response to the 2015 St. Patrick's Day storm: a global multi-instrumental overview. J Geophys Res 120(10):9023–9037. https://doi.org/10.1002/2015ja021629

Baker DN, Klimas AJ, McPherron RL, Büchner J (1990) The evolution from weak to strong geomagnetic activity: an interpretation in terms of deterministic chaos. Geophys Res Lett 17(1):41–44

Baker DN, Jaynes AN, Kanekal SG, Foster JC, Erickson PJ, Fennell JF, Blake JB, Zhao H, Li X, Elkington SR, Henderson MG, Reeves GD, Spence HE, Kletzing CA, Wygant JR (2016) Highly relativistic radiation belt electron acceleration, transport, and loss: large solar storm events of March and June 2015. J Geophys Res 121(7):6647–6660. https://doi.org/10.1002/2016JA022502

Blanc M, Richmond AD (1980) The ionospheric disturbance dynamo. J Geophys Res 85(A4):1669–1686. https://doi.org/10.1029/JA085iA04p01669

Burton RK, McPherron RL, Russell CT (1975) An empirical relationship between interplanetary conditions and Dst. J Geophys Res 80(31):4204–4214

Celebi M, Ozdemir Z, Eroglu E, Guney I (2014) Statistically defining optimal conditions of coagulation time of skim milk. J Chem Soc Pak 36(1):1–5

Chen CH, Lin CH, Matsuo T, Chen WHJ (2016) Ionosphere data assimilation modeling of 2015 St. Patrick's Day geomagnetic storm. Geophys Res 121(11):11549–11559. https://doi.org/10.1002/2016ja023346

Cherniak I, Zakharenkova I (2015) Dependence of the high-latitude plasma irregularities on the auroral activity indices: a case study of 17 March 2015 geomagnetic storm. Earth Planets Space 67:151. https://doi.org/10.1186/s40623-015-0316-x

Cherniak I, Zakharenkova I, Redmon RJ (2015) Dynamics of the high-latitude ionospheric irregularities during the 17 March 2015 St. Patrick's Day storm: ground-based GPS measurements. Sp Weather 13(9):585–597. https://doi.org/10.1002/2015sw001237

Dungey JW (1961) Interplanetary magnetic field and the auroral zones. Phys Rev Lett 6:47. https://doi.org/10.1103/PhysRevLett.6.47

Eroglu E (2018) Mathematical modeling of the moderate storm on 28 February 2008. Newast 60:33–41. https://doi.org/10.1016/j.newast.2017.10.002

Eroglu E, Aksoy S, Tretyakov OA (2012) Surplus of energy for time-domain waveguide modes. Energy Educ Sci Technol 29(1):495–506

Eroglu E, Ak N, Guney I, Sener E (2016) Component analysis of the different fish samples containing heavy metals in Istanbul Bosporus. Fresenius Environ Bull 25(1):292–299

Elliott HA, Jahn JM, David JMC (2013) The Kp index and solar wind speed relationship: insights for improving space weather forecasts. Sp Weather 11(6):339–349. https://doi.org/10.1002/swe.20053

Freund JE (1979) Modern elementary statistics, 5th edn. Prentice Hall, Arizona

Fu HS, Tu JP, Song JB Cao, Reinisch BW, Yang B (2010a) The nightside-to-dayside evolution of the inner magnetosphere: imager for magnetopause-to-aurora global exploration radio plasma imager observations. J Geophys Res 115:A04213. https://doi.org/10.1029/2009JA014668

Fu HS, Tu JJ, Cao B, Song P, Reinisch BW, Gallagher DL, Yang B (2010b) IMAGE and DMSP observations of a density trough inside the plasmasphere. J Geophys Res 115:A07227. https://doi.org/10.1029/2009JA015104

Fu HS, Khotyaintsev YV, André M, Vaivads A (2011) Fermi and betatron acceleration of suprathermal electrons behind dipolarization fronts. Geophys Res Lett 38(16):L16104. https://doi.org/10.1029/2011GL048528

Fu HS, Khotyaintsev YV, Vaivads A, André M, Huang SY (2012) Occurrence rate of earthward-propagating dipolarization fronts. Geophys Res Lett 39(10):L10101. https://doi.org/10.1029/2012GL051784
Fu HS et al (2013a) Dipolarization fronts as a consequence of transient reconnection: In situ evidence. Geophys Res Lett 40(23):6023–6027. https://doi.org/10.1002/2013GL058620
Fu HS, Khotyaintsev YV, Vaivads A, Retinò A, André M (2013b) Energetic electron acceleration by unsteady magnetic reconnection. Nat Phys 9(7):426–430. https://doi.org/10.1038/nphys2664
Fu HS et al (2014) Whistler-mode waves inside flux pileup region: structured or unstructured? J Geophys Res 119(11):9089–9100. https://doi.org/10.1002/2014JA020204
Fu HS, Vaivads A, Khotyaintsev YV, Olshevsky V, André M, Cao JB, Huang SY, Retinò A, Lapenta G (2015) How to find magnetic nulls and reconstruct field topology with MMS data? J Geophys Res Space Phys 120(5):3758–3782. https://doi.org/10.1002/2015JA021082
Fu HS, Vaivads A, Khotyaintsev YV, André M, Cao JB, Olshevsky V, Eastwood JP, Retinò A (2017) Intermittent energy dissipation by turbulent reconnection. Geophys Res Lett 44(1):37–43. https://doi.org/10.1002/2016GL071787
Gilmore M, Yu CX, Rhodes TL, Peebles WA (2002) Investigation of rescaled range analysis, the Hurst exponent, and long-time correlations in plasma turbulence. Phys Plasmas 9(4):1312. https://doi.org/10.1063/1.1459707
Gvishiani AD, Sidorov RV, Lukianova RY, Soloviev AA (2016) Geomagnetic activity during St Patrick's Day storm inferred from global and local indicators. RJES. https://doi.org/10.2205/2016es000593
Gonzalez WD, Joselyn JA, Kamide Y, Kroehl HW, Rostoker G, Tsurutani BT, Vasyliunas VM (1994) What is a geomagnetic storm? J Geophys Res 99(A4):5771–5792. https://doi.org/10.1029/93JA02867
Gonzalez WD, Tsurutani BT, Gonzalez AL (1999) Interplanetary origin of geomagnetic storms. Space Sci Rev 88:529–562. https://doi.org/10.1023/A:1005160129098
Hanslmeier A (2007) The sun and space weather, 2nd edn. In: Astrophysics and space science. Springer
Joshi NC et al (2011) Relationship between interplanetary field/plasma parameters with geomagnetic indices and their behavior during intense geomagnetic storms. Newast 16:366. https://doi.org/10.1016/j.newast.2011.01.004
Kamide Y, Yokoyama N, Gonzalez W, Tsurutani BT, Daglis IA, Brekke A, Masuda S (1998) Two-step development of geomagnetic storms. JGR Space Phys 103:6917. https://doi.org/10.1029/97JA03337
Kane RP (2010) Relationship between the geomagnetic Dst(min) and the interplanetary B_z(min) during cycle 23. Planet Space Sci 58(3):392–400. https://doi.org/10.1016/j.pss.2009.11.005
Lin J, Forbes TG (2000) Effects of reconnection on the coronal mass ejection process. J Geophys Res 105(A2):2375–2392. https://doi.org/10.1029/1999JA900477
Loewe CA, Prölss GW (1997) Classification and mean behavior of magnetic storms. J Geophys Res 102(A7):14209–14213
Manoharan PK, Subrahmanya CR, Chengalur JN (2017) Space weather and solar wind studies with OWFA. J Astrophys Astron 38:16. https://doi.org/10.1007/s12036-017-9435-z
Nava B, Zuluaga JR, Cuartas KA, Kashcheyev A, Orué YM, Radicella SM, Mazaudier CA, Fleury R (2016) Middle- and low-latitude ionosphere response to 2015 St. Patrick's Day geomagnetic storm. J Geophys Res 121(4):3421–3438. https://doi.org/10.1002/2015ja022299
Nayak C, Tsai LC, Su SY, Galkin IA, Tan ATK, Nofri E, Jamjareegulgarn P (2016) Peculiar features of the low-latitude and midlatitude ionospheric response to the St. Patrick's Day geomagnetic storm of 17 March 2015. J Geophys Res 121(8):7941–7960. https://doi.org/10.1002/2016ja022489
Rathore B, Gupta D, Parashar K (2014) Relation between solar wind parameter and geomagnetic storm condition during cycle-23. Int J Geosci. https://doi.org/10.4236/ijg.2014.513131
Saba FMM, Gonzalez WD, Gonzalez ALC (1997) Relationships between the AE, ap and Dst indices near solar minimum (1974) and at solar maximum (1979). Ann Geophys 15(10):1265–1270. https://doi.org/10.1007/s00585-997-1265-x
Sibeck DG, Lopez RE, Roelof EC (1991) Solar wind control of the magnetopause shape, location, and motion. J Geophys Res Space Phys 96(A4):5489–5495. https://doi.org/10.1029/90JA02464
Subrahmanya CR, Prasad P, Girish BS, Somashekar R, Manoharan PK, Mittal AK (2017) The receiver system for the Ooty wide field array. J Astrophys Astron 38:11. https://doi.org/10.1007/s12036-017-9434-0
Sugiura M (1964) Hourly values of the equatorial Dst for IGY, vol 35. NASA, Goddard Space Flight Center, Greenbelt, MD, p 49
Temerin M, Li X (2002) A new model for the prediction of Dst on the basis of the solar wind. J Geophys Res 107(A12):1472. https://doi.org/10.1029/2001JA007532
Temerin M, Li X (2006) Dst model for 1995–2002. J Geophys Res. https://doi.org/10.1029/2005JA011257
Tretyakov OA, Erden F (2008) Temporal cavity oscillations caused by a wide band waveform. Prog Electromagn Res B Pier B 6:183–204. https://doi.org/10.2528/PIERB08031222
Tsyganenko NA, Singer HJ, Kasper JC (2003) Storm-time distortion of the inner magnetosphere: How severe can it get? J Geophys Res 108(A5):1209. https://doi.org/10.1029/2002JA009808
Wu CC, Leping RP (2016) Relationships among geomagnetic storms, interplanetary shocks, magnetic clouds, and sunspot number during 1995–2012. Sol Phys 291(1):265–284. https://doi.org/10.1007/s11207-015-0806-9
Zic T, Vrsnak B, Temmer M (2015) Heliospheric propagation of coronal mass ejections drag-based model fitting. ApJS 218:32. https://doi.org/10.1088/0067-0049/218/2/32